JARO 10: 497–509 (2009)
DOI: 10.1007/s10162-009-0174-y
© 2009 The Author(s). This article is published with open access at Springerlink.com

JARO
Journal of the Association for Research in Otolaryngology

Dynamic Displacement of Normal and Detached Semicircular Canal Cupula

Richard D. Rabbitt,[1,3] Kathryn D. Breneman,[1] Curtis King,[4] Angela M. Yamauchi,[1] Richard Boyle,[2] and Stephen M. Highstein[3]

[1]*Department of Bioengineering, University of Utah, 72 South Central Campus Dr., Rm. 2646, Salt Lake City, UT 84112, USA*

[2]*NASA Ames Research Center, BioVIS Center, M/S 239-11, Moffett Field, CA 94035, USA*

[3]*Marine Biological Laboratory, 7 MBL Street, Woods Hole, MA 02543, USA*

[4]*EI Spectra, LLC, Woodinville, WA 98077, USA*

Received: 26 March 2009; Accepted: 4 May 2009; Online publication: 10 June 2009

ABSTRACT

The dynamic displacement of the semicircular canal cupula and modulation of afferent nerve discharge were measured simultaneously in response to physiological stimuli in vivo. The adaptation time constant (s) of normal cupulae in response to step stimuli averaged 36 s, corresponding to a mechanical lower corner frequency for sinusoidal stimuli of 0.0044 Hz. For stimuli equivalent to 40–200 deg/s of angular head velocity, the displacement gain of the central region of the cupula averaged 53 nm per deg/s. Afferents adapted more rapidly than the cupula, demonstrating the presence of a relaxation process that contributes significantly to the neural representation of angular head motions by the discharge patterns of canal afferent neurons. We also investigated changes in time constants of the cupula and afferents following detachment of the cupula at its apex—mechanical detachment that occurs in response to excessive transcupular endolymph pressure. Detached cupulae exhibited sharply reduced adaptation time constants (300 ms–3 s, n=3) and can be explained by endolymph flowing rapidly over the apex of the cupula. Partially detached cupulae reattached and normal afferent discharge patterns were recovered 5–7 h following detachment. This regeneration process may have relevance to the recovery of semicircular canal function following head trauma.

Correspondence to: Richard D. Rabbitt · Department of Bioengineering · University of Utah · 72 South Central Campus Dr., Rm. 2646, Salt Lake City, UT 84112, USA. email: r.rabbitt@utah.edu

Keywords: vestibular, inner ear micromechanics, cupula regeneration, angular motion sensation, afferent response dynamics

INTRODUCTION

The semicircular canals are responsible for sensing angular motion of the head and provide afferent signals critical to the neural control of balance, posture, and stabilization of the visual image on the retina. Biomechanics plays a key role in this process. The morphological orientation of the three canals underlies the ability to sense the direction of angular motion, and the slender geometry of the membranous duct underlies temporal integration of angular acceleration stimuli (Rabbitt et al. 2004). Each semicircular canal consists of toroidal loop of fluid including an enlarged ampulla where the sensory epithelium resides (Fig. 1). Sensory hair cell stereocilia project from the surface of the crista and into the gelatinous cupula which spans the entire cross-section of the ampulla. It is the diaphragm-like displacement of the cupula that gives rise to hair bundle displacements, mechanotransduction, and the neural response (Hillman and McLaren 1979; Markin and Hudspeth 1995; McLaren and Hillman 1979; Oman et al. 1979; Peterson et al. 1996; Rusch and Thurm 1989). A subset of semicircular canal afferents modulate their discharge rate in proportion to angular velocity of the head over a broad frequency band of physiologically relevant head movements, and hence, the canals are often described as

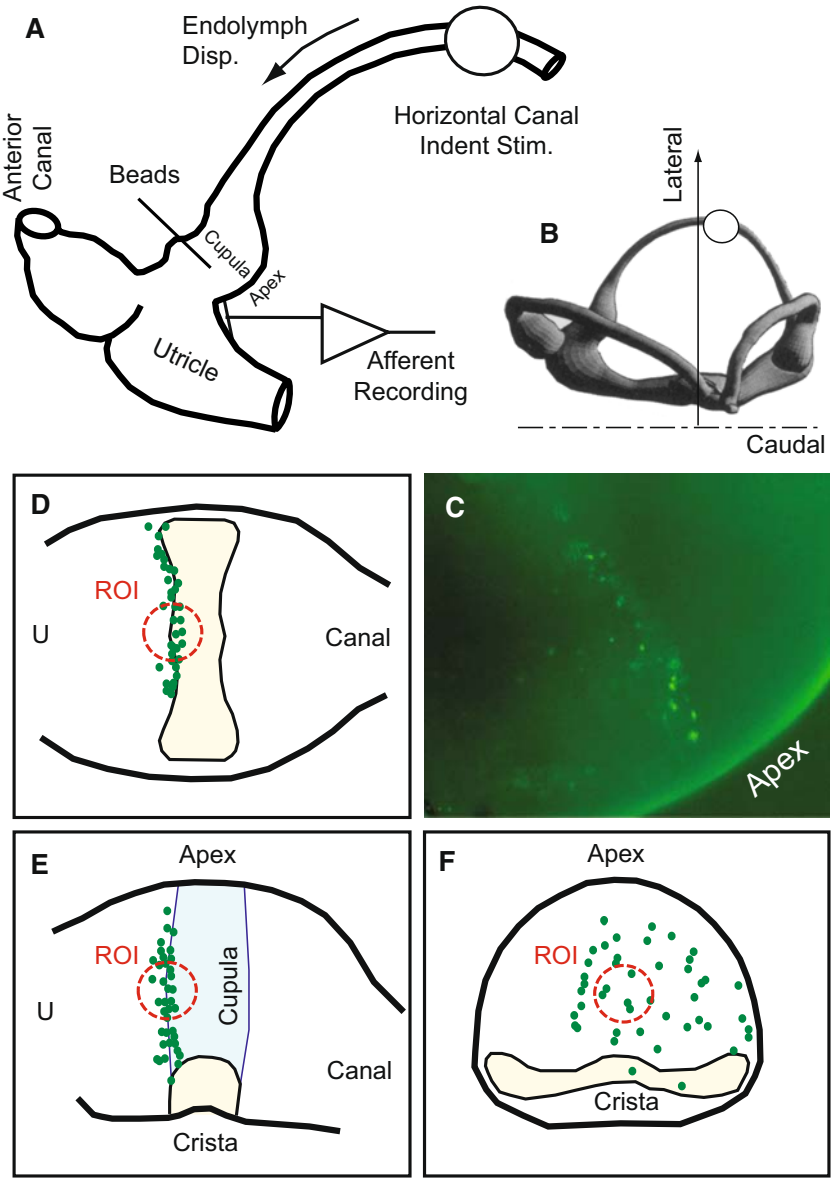

FIG. 1. Experimental setup. **A** Surgically exposed section of the labyrinth including access to the horizontal canal ampulla, membranous horizontal canal duct, and nerve branch. **B** Orientation of the membranous labyrinth as viewed from the dorsal direction. **C** Example image of fluorescent microspheres adhered to the cupula and imaged in vivo. **D–F** Orthographic projections of microspheres adhered to the cupula in one example showing a distribution and the central region of interest (*ROI*) investigated.

angular velocity sensors (Wilson and Jones 1979). From a mechanical perspective, angular velocity sensitivity arises because the viscous movement of endolymph within the slender duct causes a temporal integration of the angular acceleration stimulus, which in turn generates fluid displacements that reflect angular velocity of the head (Lorenté de Nó 1927; Oman et al. 1987; Rabbitt et al. 2004; Steinhausen 1933). This mechanical temporal integration is important because it provides the brain with a broadband angular head velocity signal that feeds into movement control neural systems including the vestibulo-ocular reflex. The primary role of the cupula is to faithfully convert fluid displacement into displacements of the mechanosensitive hair bundles. This is achieved, in part, through the elasticity of the cupula. As consequence of elasticity, the discharge modulation of velocity-sensitive canal afferent neurons is diminished and the phase is more in line with angular acceleration for angular motion stimuli below the "lower corner frequency." Theoretical considerations describe the lower corner as the frequency where the elastic restoring force of the cupula exactly balances the viscous drag of the fluid in the slender endolymphatic canal. The mechanical lower corner frequency therefore reflects the status and elasticity of the cupula as well as the viscous drag in the duct.

Here, we directly measured the adaptation time constant and lower corner frequency of semicircular

canal cupulae to physiological stimuli in the living animal while simultaneously recording individual afferent responses. Responses were measured both in normal animals and in animals with damaged cupulae (detached at the apex). The oyster toadfish, *Opsanus tau*, was used as the experimental model because of the similarity in dimensions to the human labyrinth and to facilitate the experimental approach. Results reveal the mechanical lower corner frequency to align with the lowest corner frequency of the population of velocity-sensitive afferent neurons. In a subset of experiments, we examined the motion of cupula that had become detached from the apex of the ampulla. It has been reported previously that detachment at the apex acts like a relief valve and occurs under high transcupular pressures that may arise during trauma (Hillman 1974; Rabbitt et al. 1999). The present work examined temporal responses of detached cupulae and corresponding afferents as well as the time course of reattachment and recovery of normal afferent responses.

METHODS

Animal preparation. Adult oyster toadfish (*O. tau*) were obtained from the Marine Biological Laboratory (Woods Hole, MA, USA) and all experiments were carried out under protocols approved at the Marine Biological Laboratory or the University of Utah. The surgical approach followed that described previously (Rabbitt et al. 2005). Briefly, each fish was anesthetized with MS222 (5 mg/L in seawater) and partially immobilized by an intramuscular injection of pancuronium bromide (0.05 mg/kg; Sigma, St. Louis, MO, USA) in the tail. The fish was secured in an acrylic tank, with two thirds of its body immersed in bubbled seawater, while the remainder of the body was covered with moist tissues. A craniotomy was made lateral to the dorsal course of the anterior canal to expose the horizontal canal ampulla and ~8 mm of the slender membranous labyrinth (Fig. 1B). The orientation of the labyrinth viewed from the dorsal direction (microscope objective axis) is illustrated in Figure 1A (Ghanem et al. 1998). Perilymph within the upper region of the surgical cavity was replaced with fluorocarbon (FC-75, 3 M, Minneapolis, MN, USA) to improve optical clarity and electrosurgical cutting outcomes. The electrical insulating properties of fluorocarbon allowed us to cut a fistula in the horizontal canal ampulla ~300 μm medial to the cupula using an electrosurgical generator (Valleylab, Denver, CO, USA) set to a ~5-W cutting waveform. A sharpened 76-μm dia. tungsten wire served as the cutting electrode. This generated ~50- to 100-μm diameter hole in the membranous wall allowing access for delivery of fluorescent microspheres into the endolymph (Fig. 1B, beads). The microspheres were allowed to diffuse from the fistula to the cupula. It is important to note that fluorocarbon is immiscible with endolymph, and as a result, there was a surface tension barrier preventing flow of endolymph out of the fistula (Rajguru and Rabbitt 2007). Canal afferent responses to controlled stimuli were recorded after generation of the fistula and compared to control recordings to confirm normal sensory transduction and neural coding, indicating that the dynamics are indeed dominated by the long and slender canal segment.

Although great effort was taken to prevent damage to the cupula during this procedure, in a subset of animals, we found afferent modulation to be reduced, and in some cases, we observed a fraction of the fluorescent microspheres to diffuse over the apex of the cupula and into the lateral side of the ampulla. These animals defined the "dislodged cupula" group. Even in these damaged cases, the cupula remained structurally sound, but simply detached from the interior surface of the membranous ampulla at its apex. Present results address cupula responses and reattachment in modestly damaged cases where the cupula was dislodged at the apex but remained located in the normal central region of the ampulla.

Mechanical stimulus. Mechanical indentation of the slender limb of the membranous duct was used as the primary stimulus. This idea was first introduced by Ewald in 1892 (Camis 1930) and later refined by Dickman et al. to mimic physiological head movements and produce nearly equivalent afferent discharge patterns (Dickman and Correia 1989; Dickman et al. 1988). We used a version of the approach detailed by Rabbitt et al. (1995) where 1 μm of mechanical indentation of the horizontal canal limb generates mechanical cupula motion and afferent responses nearly equivalent to ~4 deg/s of angular head velocity stimulus in the present experimental organism. In a subset of experiments, the whole animal was rotated using sinusoidal angular velocity stimuli (Boyle and Highstein 1990). Cupula displacements were recorded for mechanical indentation stimuli, but not for angular velocity stimuli.

Neural recordings. Horizontal canal neural recordings used glass microelectrodes (~100 MΩ) following the approach described previously (Boyle and Highstein 1990; Rabbitt et al. 2005). Electrodes were positioned using a micromanipulator at a location ~500 μm from the horizontal canal ampulla where the nerve branch is accessible (Fig. 1B). Extracellular potentials were measured using standard amplification (EXT-02F, npi electronic, Tamm, Germany). Afferent responses and

mechanical stimuli were amplified, filtered at 2 kHz (LHBF-48X, npi electronic), and sampled at 5 kHz (ITC-18, HEKA Instruments, Inc., Bellmore, NY, USA).

Microspheres. Carboxylate-modified, neutrally buoyant fluorescent microspheres (beads) were obtained (Bangs Labs, Inc. Fishers, IN, USA) and surface-modified to bind wheat germ agglutinin (WGA). Raw beads in suspension were washed twice in MES buffer with 10 mg EDAC and incubated for 15 min. Following incubation, the beads were washed and resuspended in 0.1 M borate buffer (pH 8.5) with 1 mg WGA (Sigma-Aldrich) and incubated with gentle mixing for 4 h. The beads were then washed and resuspended in 0.1 M borate buffer with bovine serum albumin (BSA; 10 mg/mL) and mixed continuously for 15 min prior to a final wash and resuspension in MES buffer with BSA (10 mg/mL) for storage. Microspheres were placed in toadfish artificial endolymph (Ghanem et al. 2008), vortex-mixed, and loaded into a glass pipette pulled and cut to ~50-μm tip diameter. The fluid level in the pipette was adjusted to just exceed the capillary action of the glass. The filled pipette was then lowered through the fluorocarbon until the tip contacted the endolymph through the fistula in the ampulla membrane. Contact with endolymph caused the surface tension between the endolymph and the fluorocarbon to be broken and placed the interior of the pipette in communication with the endolymph. Microspheres were allowed to diffuse out of the pipette and into the ampulla. Over time, some of the beads migrated to the cupula and adhered to its surface. The microsphere loading pipette was removed prior to collecting any data.

Fluorescent microsphere tracking. Images were collected using an upright microscope (Axioskop Tech, Carl Zeiss, Germany) configured for epifluorescence and placed on a vibration isolation table (TMC, Peabody, MA, USA). Long working distance air 5×, 10×, 20× objectives (Plan Apo, Mitutyo, Japan) were used to view the complete ampulla, fluorescent microbeads, and the neural recording electrode. A CCD camera (Retiga-EXi, QImaging, Surrey, BC, Canada) was used to collect fluorescent images at a frame rate of ~100 ms and exposure time of ~50 ms. Shutter times were sampled and recorded. Custom software was written (Igor Pro, Wave Metrics, Lake Oswego, OR, USA) to control the stimuli (NI GPIB, National Instruments, Austin, TX, USA), trigger the camera, and to collect the neural data, image data, and stimuli via computer (Apple G4, Cupertino, CA, USA; ITC-18, HEKA Instruments, Inc.). Images (1392×1040) were collected over two to ten cycles of periodic mechanical indentation stimuli with shutter times random relative to the stimulus period. Images were time-stamped relative to the stimulus onset trigger over multiple applications of the stimulus and subsequently combined. Since image sampling was random relative to the periodic stimulus, data collected over several cycles provided temporal resolution of ~50 ms with respect to the stimulus timing trigger.

Figure 1C shows an example image of fluorescent microspheres adhered to the cupula, imaged in the living animal. It was straightforward to estimate the three-dimensional locations of the beads by adjusting the "*Z*"-axis focus and manually digitizing the centroids of the microspheres from still images. An example showing the distribution of fluorescent microspheres in one animal is provided as orthographic projections in Figure 1D–F. Specific locations and numbers of microspheres adhered to the cupula varied substantially between individual animals. Typically, ten to 50 microspheres adhered to the cupula, with five to 20 located on the central region of interest (ROI). Results reported in the present study are limited to motion of beads in the ROI located near the center of the cupula (Fig. 1, dotted circular), on the central pillar overlaying the center region of the crista (Silver et al. 1998).

Motion of the cupula was tracked by focusing on a subset of fluorescent microspheres located in the ROI and collecting a sequence of ~300 images while presenting multiple applications of the mechanical indentation stimulus. Since the animal was alive, there were always slight whole organ movements caused by respiration, heartbeat, or random muscle contractions. To remove these movement artifacts, we manually selected image registration ROIs at the apex of the ampulla and at the crista, being careful that the registration ROIs did not include any microspheres adhered to the surface of the cupula. The first image in the sequence was used as the reference configuration. The registration ROIs of all subsequent images were then aligned with the reference image using the approach of (Thévenaz and Unser 1998), as implemented by Wave Metrics (Igor Pro 6, Lake Oswego, OR, USA). All images in the sequence were translated and rotated to align the registration ROIs with the reference configuration. After registration of all images, the same approach of Thévanaz and Unser was applied to track motion of the microspheres 20×20 pixel square ROI around each bead intensity centroid. Beads within the ROI were selected manually and the intensity centroid was found using custom software (Igor Pro 6, Wave Metrics). Analysis of microspheres adhered to the membranous labyrinth (ampulla) resulted in motions <200 nm, thus suggesting a noise floor of <200 nm—a value that could be improved by averaging over multiple stimulus presentations if desired. The present study

used stimuli producing motions an order of magnitude above this noise level, and therefore, averaging was not required. To track cupula motion, five to ten microspheres within the central ROI were selected and tracked individually. The procedure resulted in microsphere displacements in the "*x*–*y*" coordinate frame of the CCD array. These data were combined to determine the component of motion perpendicular to the surface of the cupula, with the surface tangent identified by the group of fluorescent beads.

RESULTS

Sinusoidal mechanical indentation of the canal duct produced afferent responses consistent with previous reports in this species (Rabbitt et al. 1995). Figure 2 provides example simultaneous recordings of single-unit afferent discharge (A) and cupula displacement (B) in response to ~20-μm mechanical indentation of the canal duct at 0.3 Hz. As expected, cupula displacement was in phase with mechanical indentation, and since indentation mimics head rotation (Dickman and Correia 1989), cupula displacement would be in phase with angular velocity of the head. The magnitude was ~4 μm in this animal which corresponds to a cupular gain in the central ROI of ~50 nm per deg/s of angular head velocity. The average cupula gain was 53 nm per deg/s (n=9; 13 nm SE; 4 deg/s rotation ~ 1 μm indent), consistent with the previous report by (McLaren and Hillman 1979) of ~35 nm per deg/s. In contrast to this previous work, we found displacement of the cupula to be in phase with the mechanical stimulus and angular head velocity, at least at frequencies above the lower corner where many afferent neurons encode angular head velocity (e.g., Fig. 2B, C). For indentation stimuli 10–24 μm in amplitude, harmonic distortion of the cupula displacement was less than 15% and the first harmonic was nearly linear, with stimulus amplitude yielding Pearson's R=0.86. A subset of afferents exhibited a much higher degree of harmonic distortion due primarily to an excitatory–inhibitory asymmetry in afferent discharge response dynamics. Four additional example afferent responses to the 0.3-Hz stimulus are shown in the bottom panels (Fig. 2D). Angular velocity (vel.) encoding units responded with a maximum discharge rate in phase with the peak displacement of the cupula. The response gain of these units was relatively insensitive to stimulus frequency. A subset of afferent units responded with a phase advance and increased gain with frequency—a response that encodes angular acceleration (accel.) of the head. These acceleration-sensitive units are not present in all species. In the toadfish, convergence of both excitatory and inhibitory transmitters appears to underlie a mathematical differentiation of cupula displacement to arrive at acceleration-sensitive afferent discharge patterns (Holstein et al. 2004).

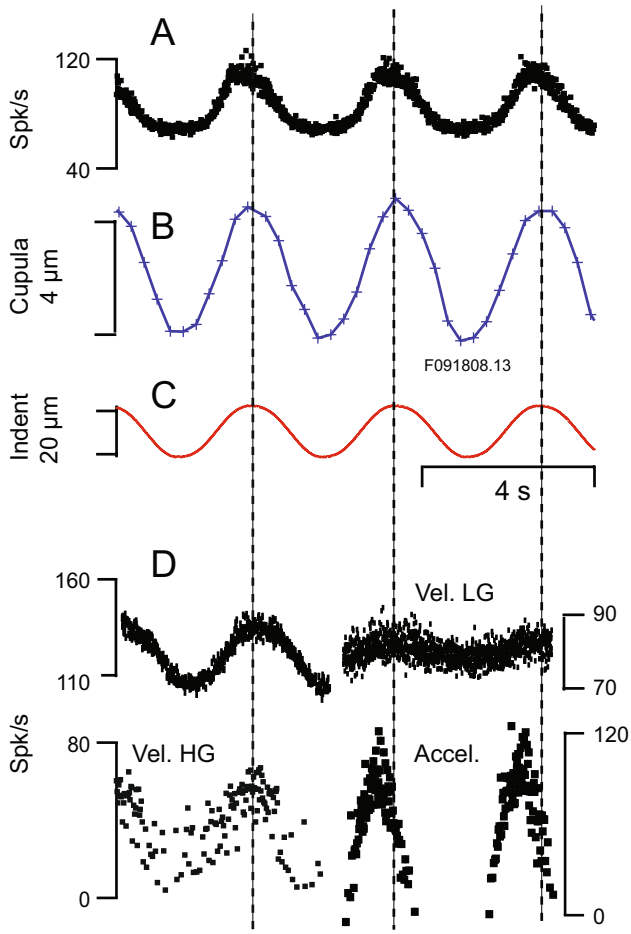

FIG. 2. Cupula displacement and afferent responses to 0.3-Hz sinusoidal stimuli in normal animals. Simultaneous recordings of afferent responses (**A**) and cupula displacement (**B**) in response to sinusoidal stimulus (**C**) at 0.3 Hz. **D** Additional afferents recorded in response to the same stimulus showed a range of gains and relative phases of peak response. Since 0.3 Hz is above the mechanical lower corner frequency, a subset of afferents responded in phase with, and in proportion to, cupula displacement (velocity-sensitive), while other afferents responded with a phase advance relative to cupula displacement (e.g., acceleration-sensitive).

In order to investigate dynamics of cupula displacement, we used step indentation of the canal duct. Step indentation evoked a rapid displacement of the cupula toward the utricle followed by a slow recovery (adaptation) to its resting position. Figure 3 shows simultaneous recordings of horizontal canal afferent discharge patterns (A, D, G), and displacements of fluorescent microbeads attached to the cupula (B, E, H), in response to square wave (C, F, I) mechanical indentation of the canal duct (three example animals). During excitatory step stimuli, afferents quickly increased their discharge rate followed by a period of

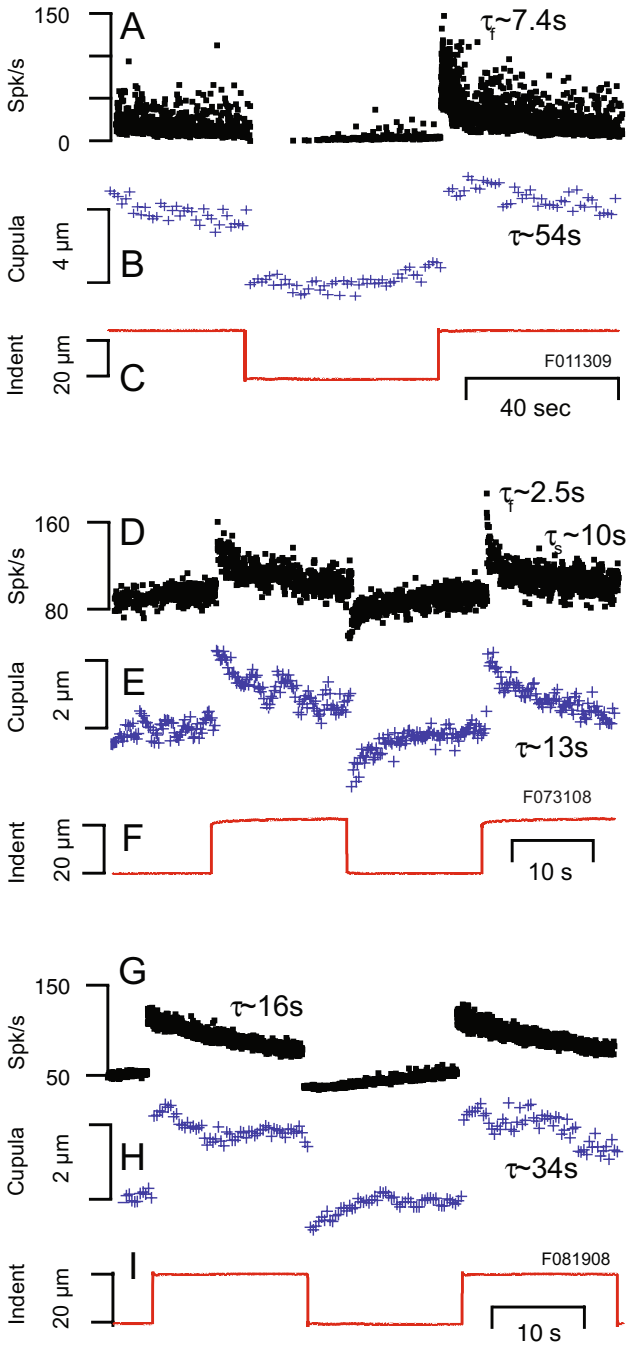

FIG. 3. Cupula displacement and afferent time constants in normal animals. Simultaneous recordings of afferent responses (**A**, **D**, **G**) and cupulae deflections (**B**, **E**, **H**) in response to square wave mechanical indentation (**C**, **F**, **I**) of the canal duct for three different animals. Cupula deflections in the central ROI were 3–6 μm for duct indentations of 20 μm, and cupula time constants for the units in this figure were τ=13–54 s. Afferent response time constants were less than cupula time constants due to adaptive processes in the hair cell/afferent complex.

recovery back to their background discharge. Slowly adapting afferents encode angular velocity over a broad frequency band of sinusoidal stimuli and are analogous to the regularly discharging units in mammals (Fernández and Goldberg 1971; Goldberg and Fernandez 1971; Rabbitt et al. 2005). The most rapidly adapting afferents encode angular acceleration of the head, also over a broadband. For step stimuli, some afferents recovered following a single exponential, while others recovered following a fast adaptation, τ_f, followed by a slow adaptation, τ_s. The fast component of afferent adaptation, if present during excitatory stimuli, was absent or greatly reduced during inhibitory stimuli. This asymmetry was not obvious in the motion of the cupula (B, E, H), which deflected with nearly equal time courses for both excitatory and inhibitory stimuli for the magnitudes of stimuli investigated here. For sinusoidal stimuli above the mechanical lower corner frequency ($\omega > 1/\tau$ rad/s), the cupula deflected in proportion to, and in phase with, the stimulus (Fig. 2, peak cupula displacement B aligns with stimulus C).

Adaptation of the cupula following step indentation of the duct is more clearly demonstrated in Figure 4A where multiple stimulus cycles are overlaid and fit with exponential curves (solid curves). The time constant of cupula adaptation averaged $t \sim 36$ s (n=9), but varied considerably between individual animals (13–104 s, Fig. 3C). Fluorescent microbeads within the central ROI of each animal moved together with nearly the same time constant, thus suggesting that the range of cupular time constants was primarily due to interanimal variability and not spatial distribution of beads. The present study did not investigate the deflected shape of the cupula or if differences in the time constant could be detected at different locations. All of the animals were of nearly the same size, and therefore, it seems unlikely that differences between mechanical time constants between animals could be explained by morphology alone. Although we cannot rule out variations in the diameter of the membranous duct as underlying interanimal variability, it seems likely that the mechanical properties of cupulae may differ between individual animals, with rapidly adapting cases being stiffer and/or more permeable than slowly adapting cases.

Mechanical indentation of the membranous labyrinth is known to lead to large transcupular pressures and, if the stimulus is excessive, can detach the cupula at its apex (Hillman 1974; Rabbitt et al. 1999). Although we did not intend to damage the cupula, in several cases, the cupula became detached during preparation of the animal. Detached cupulae showed a diverse range of motions depending on the extent of damage. Afferent responses, if present, reflected this diversity. In the most severe detachment cases, the cupula would swing toward the utricle, leaving a gaping opening for endolymph to flow over its apex from the canal lumen into the utricular vestibule. The cupula always remained attached to the sensory

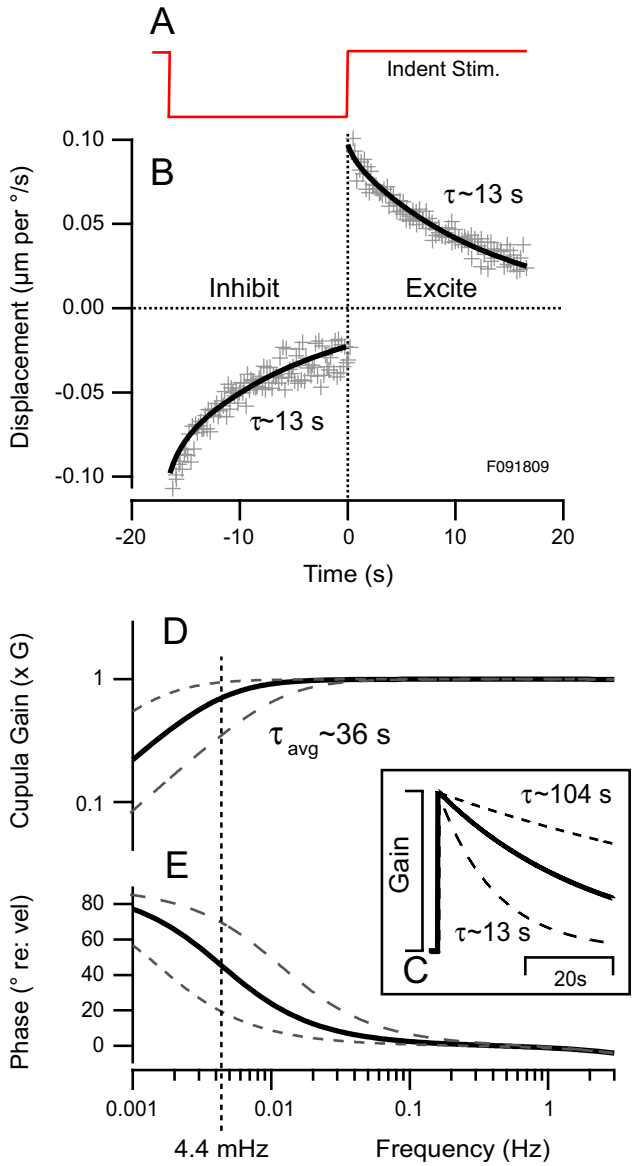

FIG. 4. Cupula time constants. **A** Mechanical indentation stimulus. **B** Overlay of data from several repeated stimuli presentations with images collected at random times relative to the stimulus to maximize temporal resolution. Using indentation stimuli to mimic angular rotation, the gain of cupula deflection in this particular animal was $G \sim 0.09$ μm per deg/s of angular head velocity and the slow time constant associated with the lower corner frequency of the canal was 13 s. Over all animals tested, the gain averaged $G = 0.08$ μm per deg/s and the adaptation time constant in response to step stimuli averaged $\tau \sim 36$ s ($n = 10$). **C** The range of time constants observed (13–104 s). **D–E** Bode plots showing the gain and phase of cupula displacement for sinusoidal stimuli predicted from the time constants measured here using step stimuli.

epithelium with an orientation perpendicular to the sensory epithelium and aligned with the hair bundles, thus showing a much stronger attachment at the base vs. a weak attachment at the apex. Grossly dislodged cupulae did not respond to mechanical indentation of the slender duct, at least within the limits of our experimental setup. Consistent with this, afferents in these damaged organs did not modulate in response to angular rotation of the animal or mechanical indentation of the duct. This is not surprising since the fluid pressure drop across a grossly dislodged cupula would approach zero.

In three animals, we observed reattachment of the cupula and recovery of normal afferent discharge responses to mechanical stimuli ~7 h after the initial damage. Recovery of function occurred in cases where the cupula was dislodged at its apex but oriented properly within the ampulla. Presumably, more severely damaged cupula would take much longer to recover. In the modestly detached cases reported here, the apex of the cupula was observed to slide along the inside surface of the ampulla during mechanical indentation stimuli. The cupula did not return completely to its initial position after cessation of the stimulus. When detached, motion of the cupula at the surface of sensory epithelium was very small relative to motion at the apex, and hence, afferent modulation was reduced or absent. The displaced shape of the dislodged cupula was similar to a cantilever beam with the base firmly secured to the sensory epithelium and the apex free to swing under the ampullary apex.

Figure 5 shows cupulae displacements and afferent responses recorded from two animals with damaged cupulae. In panel B, notice that the time constant of the cupula is drastically reduced relative to normal controls (e.g., 1.4 s in this animal vs. normal in Figs. 3 and 4). Like the control condition when the canal duct was rapidly indented, an excitatory transcupular pressure was immediately generated and this compelled a rapid displacement of the cupula toward the utricle. Unlike the control condition, the pressure was quickly relieved and the cupula rapidly returned to its resting position as the endolymph flowed over the detached apex of the cupula and into the utricular vestibule. This decreased time constant can be understood by a simple model that accounts for the leakage flow over the apex (see Appendix). Consistent with the reduced time constant of the cupula, the afferents also showed reduced time constants (arrows, Fig. 5A). Afferent time constants were always less than the cupula time constant. Again, like controls, there was an excitatory–inhibitory asymmetry in afferent responses that was not present in the cupula displacement (panel A vs. B). In one animal, we captured records while the cupula was in the process of reattachment, approximately 5 h after damage (Fig. 5D–F). When deflected in the excitatory direction, the cupula in this animal deflected like controls (Fig. 5E) and afferent modulation was normal (Fig. 5D). In contrast, inhibitory stimuli momentarily detached the cupula and resulted in a very fast

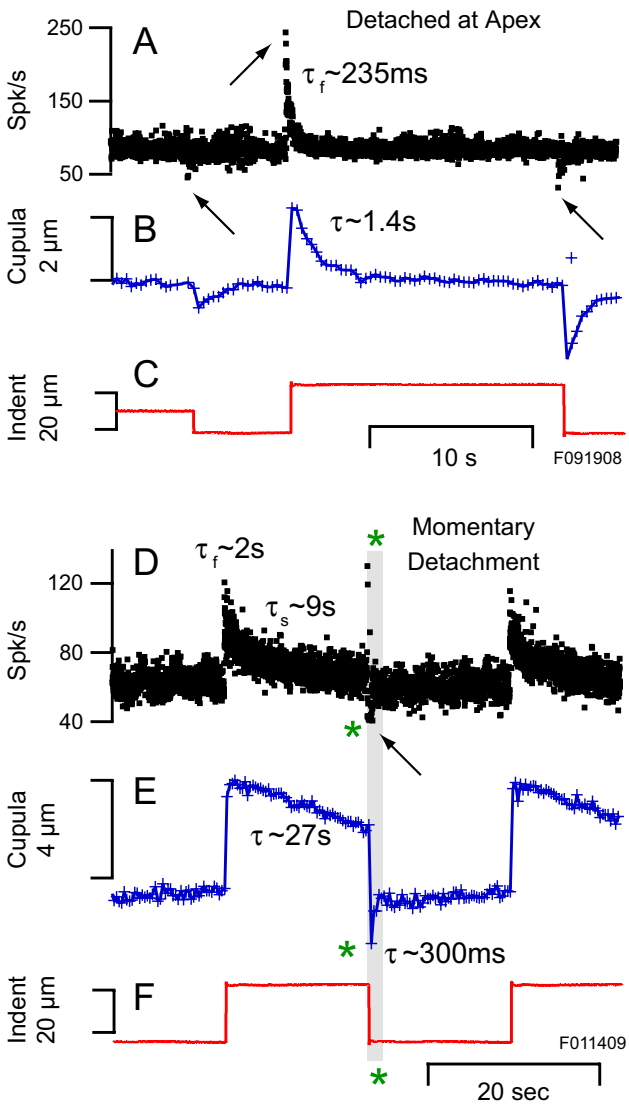

FIG. 5. Displacement and afferent responses with a dislodged cupula. **A–C** Data from organ with cupula detached at its apex showing rapid adaptation of cupula displacement (**B**) re: controls (Figs. 2 and 3) and rapid adaptation of afferent responses (**A**). **D–F** Partially recovered cupula showing normal attached responses during excitatory stimuli but detached responses during the inhibitory phase.

cupular time constant (Fig. 5E, asterisk) and corresponding rapid afferent adaptation (Fig. 5D, asterisk). These data show that the cupula was attached for excitatory stimuli but detached for inhibitory stimuli, suggesting a stick–slip behavior. After 7 h, the inhibitory detachment disappeared and responses fell within the range of control animals (e.g., Fig. 3). Reattachment of the cupula over time is further shown in Figure 6. A ~10-µm step indentation of the canal was used as the stimulus (Fig. 6A), corresponding to approximately 40 deg/s step increase in excitatory angular velocity of the head. In the dislodged case (Fig. 6B, curve "a"), the cupula underwent rapid displacement toward the utricle just like normal controls (expanded in Fig. 6C), but unlike the control condition, the deflection quickly returned back to a resting position. The time constant of the rapid mechanical adaptation was ~300 ms in this animal. It is significant to note that the cupula did not return entirely to its original position at the end of the stimulus (Fig. 6C). This "offset" was accompanied by sliding of the cupula along the inside surface of the ampulla, and presumably, the offset was maintained by loose adhesion of the cupula to the ampulla and is consistent with the stick–slip behavior described above. The sliding was not obvious in all detached cupulae (e.g., Fig. 5B), nor was it observed in the normal intact condition.

The two rapidly adapting records in Figure 6C were recorded from the same animal ~1 h (red) and ~4.5 h (blue) after damage to the cupula. Results at these two time points were virtually identical, indicating that the regeneration process had not yet reached the apex of the cupula where reattachment was necessary. After ~7 h (Fig. 6B, curve "b"), the cupula had reattached at its apex and exhibited an adaptation time constant of ~27 s, consistent with the time constants in control recordings. The time constant did not change at later time points (curve "c", 10 h), but a drop in gain sometimes occurred due to loss in preload of the indentation stimulus over time (Rabbitt et al. 1995). We did not observe intermediate stages of cupula recovery, suggesting that reattachment process may be quick once the appropriate extracellular adhesion molecules are delivered to the apex.

In a singular case, we opened the cranial cavity to discover an ampulla containing two cupulae. One cupula was slightly discolored light brown, dislodged, and tilted toward the utricle, while the other cupula was pristine, transparent, and in the standard position (schematic Fig. 7A). The two cupulae interpenetrated each other at their connection to the sensory epithelium. The pristine transparent cupula was presumed to be a regenerated replacement for the dislodged cupula. There was no sign of damage to the cranial cavity or other prior injury to the animal. It was not possible at the time to record cupula motion or indent the canal, but we were able to record horizontal canal afferent modulation to sinusoidal whole body rotation in this animal. Results are shown in Bode form of gain (Fig. 7B, spk/s per deg/s) and phase (Fig. 7C, deg, re: peak angular velocity) and compared to a population of control animals reported by Boyle and Highstein (1990). Square symbols show afferent responses for the regenerated cupula (fit with thick black lines), while small symbols show three groups of control afferents in the same species. Responses in the regenerated cupula animal were phase advanced re: velocity, had lower gains, and exhibited more increase in gain with frequency than

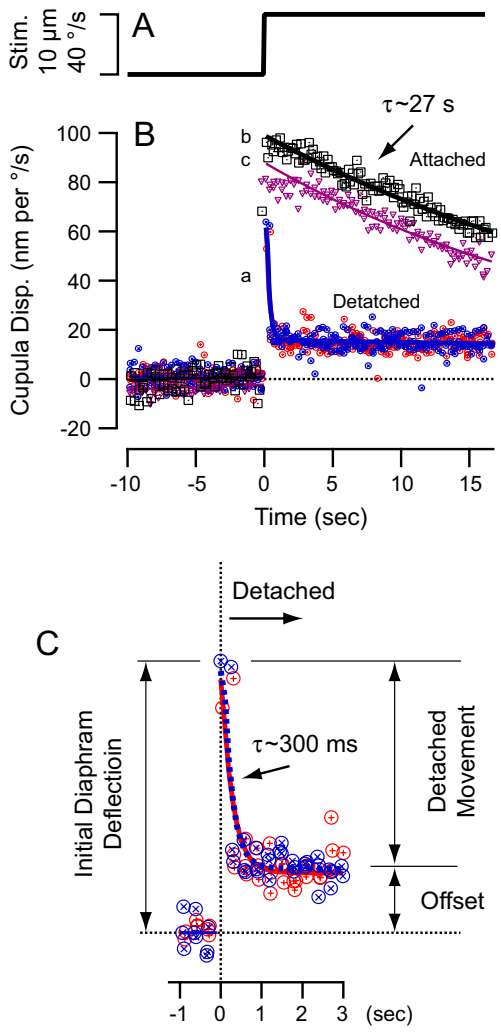

FIG. 6. Reattachment the cupula. **A** Step mechanical indentation stimulus generating a pulse of endolymph flow toward the ampulla and transcupular pressure. **B** Displacement of the cupula when damaged (*a*) showing rapid adaptation followed by a maintained offset position. After ~6 h, the cupula recovered and exhibited the normal slow adaptation (*b, c*) associated with the elasticity of the cupula slowly pushing the endolymph back into the canal duct (τ~ 27 s). **C** Expanded view for the damaged cupula showing immediate deflection of the cupula followed by rapid adaptation as endolymph flowed over its apex. Cupula adaptation was τ~300 ms in this case.

most control afferents. The gain did approach average controls as the frequency exceeded 1 Hz, but the phase remained abnormally advanced. It was confirmed by dye injection that the regenerated cupula was attached at the apex. It was further confirmed after the experiment that both cupulae were neutrally buoyant in endolymph, and therefore, the density of the cupula could be ruled out as a factor contributing to the change in afferent response dynamics. The source of the change in response dynamics is not known, but it is possible that the regeneration of the cupula was not complete and that it was leaky or more permeable to endolymph than normal. Based on the simple analysis in the Appendix, increased permeability could account for the data, but it is also possible that non-mechanical factors were at play. The implication of complete cupula regeneration raises numerous questions about how, and under what conditions, this avascular extracellular reconstruction is accomplished.

DISCUSSION

The average adaptation time constant of the cupula measured in normal animals was 36 s and the average gain was 53 nm per deg/s of angular head velocity. It

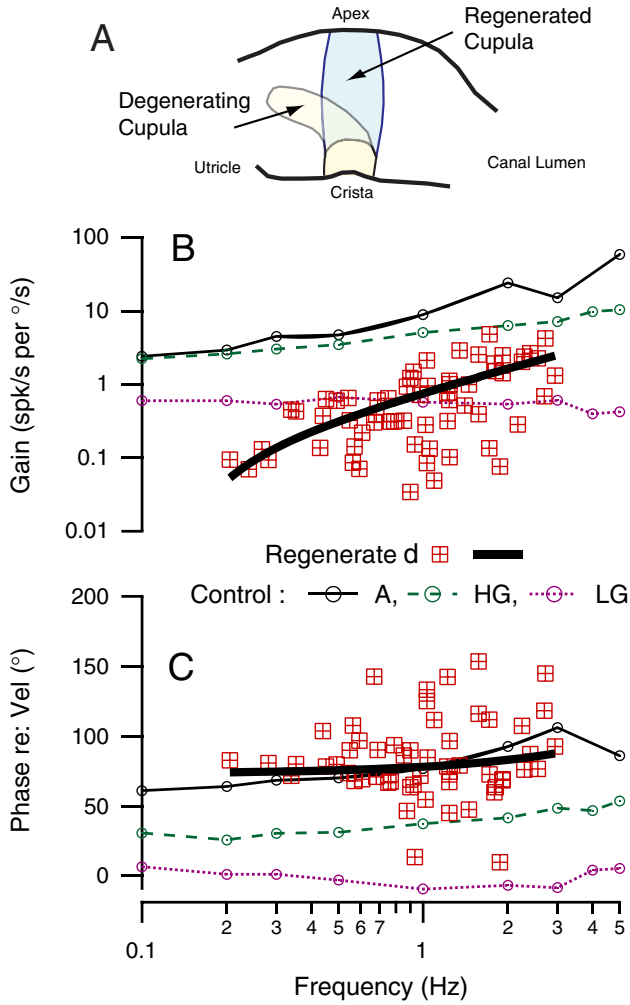

FIG. 7. Regeneration of the cupula. **A** Sketch showing observation in one animal of a degenerating cupula displaced toward the utricle and a second regenerated cupula spanning the cross-section of the ampulla. Bode plots showing the gain (**B**) and the phase (**C**) of a population of single afferent units in response to sinusoidal angular rotation of the whole animal in comparison to control recordings from a population of normal animals from Boyle and Highstein (1990). Afferent responses did not span the normal range and were biased toward high phase advance (**C**) and low gain (**B**).

has been shown previously that step stimuli (Rabbitt et al. 2005), or more complex waveforms (Paulin et al. 2004), can be used to estimate frequency domain responses of vestibular afferents. This nearly linear behavior allows us to use the time constant for step stimuli measured here to predict the mechanical lower corner frequency for sinusoidal angular motion of the head to be ~0.0044 Hz ($\omega=1/\tau$ rad/s). Physically, the mechanical lower corner occurs at the frequency where the viscous drag force of endolymph balances the elastic restoring force of the cupula (Oman et al. 1987; Rabbitt et al. 2004; Steinhausen 1933; Van Buskirk 1987). Above the lower corner frequency, present data confirm that the biomechanics of the semicircular canals serves to integrate the angular acceleration stimuli to generate cupular displacements that are proportional to and in phase with angular velocity of the head (valid at least up to the 10 Hz Nyquist frequency of the present image acquisition approach). For angular motion stimuli below the lower corner frequency, the gain of the cupula is attenuated and the phase is advanced re: angular velocity. This is illustrated in Figure 4 in the Bode form of gain (D) and phase (E). We also used the mechanical time constant to estimate the elasticity of the cupula. This estimate used the viscosity of endolymph (Steer et al. 1967) and the morphology of the toadfish labyrinth (Ghanem et al. 1998), combined with Eqs. 3, 6, and 11 (Appendix) to estimate a cupula elastic shear modulus of ~0.12 N/m^2 (1.2 dyn/cm^2).

Across the experimental population, afferents adapted more rapidly than the cupulae in the same animals, thus showing that adaptation to step stimuli (and the lower corner frequency observed for sinusoidal rotation) does not directly reflect displacement of the cupula but also includes adaptive properties of hair cell/afferent complexes. Although there are differences between species, there is no doubt that the hair cell/afferent complexes contribute additional signal processing beyond mechanical inputs that shape afferent responses (Anastasio et al. 1985; Baird et al. 1988; Boyle and Highstein 1990; Brichta and Goldberg 1996; Ezure et al. 1978; Fernández and Goldberg 1971; O'Leary and Honrubia 1976; Peterka and Tomko 1984; Curthoys 1982). This may explain why morphologically based mechanical models of canal function do not describe responses of all afferents (Hullar 2006). Cupular adaptation time constants reported here in normal control animals were recorded near the center of each cupula, on the surface facing the utricular vestibule. This part of the cupula overlies the region of the sensory epithelium innervated by the most rapidly adapting afferents in this species (Boyle et al. 1991; Boyle and Highstein 1990), thus highlighting the difference between the slowly adapting cupula and more rapidly adapting afferents. The decreased mechanical adaptation time constants reported here for dislodged cupula were pathological and cannot explain diversity of afferent adaptation times observed within individual animals under healthy conditions. We did not investigate regional variability in the present study, and it remains possible that different regions of the cupula might adapt with different time constants. It also remains possible that motion of the sensory hair bundles might not occur in perfect step with displacement of the cupula. These hypothetical mechanical explanations for differences between afferent discharge vs. cupula motion, however, seem unlikely given all the data at hand. Rather, present results for normal intact cupulae are consistent with previous reports attributing the diversity in afferent adaptation properties primarily to non-mechanical factors (Highstein et al. 2005; Lysakowski and Goldberg 2003; Rabbitt et al. 2005).

Normally, the cupula is attached around its entire perimeter, occludes the complete cross-section of the ampulla, and prevents endolymph from flowing past (Hillman and McLaren 1979; McLaren and Hillman 1979). In a subset of experiments reported here, the cupula had become detached at its apex, thus allowing endolymph to flow in the restricted space between the cupula and the apex of the ampulla. These animals did not manifest obvious vestibular symptoms prior to the experiment, suggesting that cupula detachment likely occurred during the surgical procedure. The condition was consistent with earlier reports describing cupula detachment resulting from high transcupular pressures induced by mechanical trauma or rapid deformation of the membranous labyrinth (Hillman 1974; Rabbitt et al. 1999). When detached modestly at the apex, cupulae and afferents still responded but with abnormally reduced low-frequency gains and much faster adaptation time constants. This can be understood by endolymph leakage over the apex (e.g., Figs. 5 and 6 and Appendix). Reattachment was observed to occur abruptly after about 5–7 h, consistent with the hypothesis that extracellular adhesive molecules arrived at the damaged apex of the cupula after this period of time. The molecular cell biology of this process is unknown, but may involve up-regulation of cupula generation by supporting cells in the crista (Anniko and Nordemar 1982) and the subsequent transport time from the crista to the apex.

ACKNOWLEDGMENTS

Financial support was provided by the NIDCD R01 DC06685 (Rabbitt) and NASA GSRP 56000135 & NSF IGERT DGE-9987616 (Breneman).

Open Access

This article is distributed under the terms of the Creative Commons Attribution Noncommercial License which permits any noncommercial use, distribution, and reproduction in any medium, provided the original author(s) and source are credited.

APPENDIX: ONE-DIMENSIONAL MODEL

Present experimental results show that the cupula adapts much more rapidly after it has been partially detached from the ampullary membrane at its apex. The reduced adaptation time occurs because the endolymph is allowed to flow over the apex of the cupula instead of around the entire endolymphatic duct. We can understand the basic principle using a simple one-canal model of the fluid mechanics (Oman et al. 1987; Rabbitt et al. 2004) modified to allow fluid flow through the cupula (Damiano 1999; Rabbitt 1999). In the simplest analysis, endolymph volume displacement, Q_e, is governed by a second-order equation:

$$m\frac{d^2Q_e}{dt^2} + c\frac{dQ_e}{dt} = \ddot{\Omega}f - \Delta P \tag{1}$$

where $\ddot{\Omega}$ (rad/s^2) is the angular acceleration of the skull and ΔP is the pressure drop across the cupula. The effective mass (m) and damping (c) coefficients arising from the endolymph fluid mechanics in the slender duct are given approximately by (Rabbitt et al. 2004):

$$m \approx \frac{\rho\ell}{A_d} \tag{2}$$

$$c \approx \frac{8\pi\mu\ell}{A_d^2} \tag{3}$$

and the forcing coefficient arising from the inertial mass of the accelerating endolymph is:

$$f = 2\pi\rho R^2\cos(\vartheta). \tag{4}$$

In these expressions, ρ is the endolymph density, μ is the endolymph viscosity, ℓ is the length of the slender portion of the endolymphatic duct measured along its curved centerline, $A_d{=}\pi r^2$ is the cross-sectional area of the slender endolymphatic duct, R is the radius of curvature of the toroidal canal, and ϑ is the angle between the plane of rotation and plane of the canal. In the simplest case, the volume displacement of the cupula, Q_c, is approximated using:

$$kQ_c = \Delta P \tag{5}$$

where the volumetric stiffness, k, is approximated by:

$$k \approx \frac{8\pi\gamma h}{A_c^2}. \tag{6}$$

In this, γ is the elastic shear stiffness of the cupula, h is its thickness, and A_c is the cross-sectional area of the ampulla spanned by the cupula. We have assumed that partial detachment has not compromised the stiffness. We also assume that viscous leakage around the detached cupula is governed by Stokes flow, so the relative volume flow between the endolymph and cupula is related to the pressure drop across the cupula according to:

$$\Delta P = \Gamma\left(\frac{dQ_e}{dt} - \frac{dQ_c}{dt}\right) \tag{7}$$

where Γ is the Stokes hydraulic resistance associated with the dislodged gap between the cupula and the ampulla wall. Combining equations, the volume displacement of the cupula is approximated by:

$$m^*\frac{d^2Q_c}{dt^2} + c^*\frac{dQ_c}{dt} + k^*Q_c = \ddot{\Omega}f \tag{8}$$

where the new damping and stiffness coefficients accounting for leak past the cupula are:

$$c^* = c + mk/\Gamma \tag{9}$$

and

$$k^* = k(1 + c/\Gamma). \tag{10}$$

With this, the slow time constant governing adaptation of the cupula is:

$$\tau_1 \sim \frac{c^*}{k^*} = \frac{c + mk/\Gamma}{k + ck/\Gamma} \tag{11}$$

and the fast time constant governing onset transients is:

$$\tau_2 \sim \frac{m^*}{c^*} = \frac{m}{c + mk/\Gamma}. \tag{12}$$

We note that this model reduces to the standard model as the hydraulic resistance preventing endolymph leakage around the dislodged cupula becomes large, i.e., as $\Gamma\to\infty$. For a step angular velocity of the head of magnitude $\dot{\Omega}$ (rad/s), the cupula volume displacement predicted by this simple model follows the time course:

$$Q_c(t) = \frac{\dot{\Omega}f\tau_1\tau_2}{m(\tau_1 - \tau_2)}\left(e^{-t/\tau_1} - e^{-t/\tau_2}\right). \tag{13}$$

This expression can also be used to estimate cupula volume displacements in response to mechanical

indentation by noting that 1-μm indentation is equivalent to approximately 4 deg/s (0.07 rad/s) of angular head velocity. For the current experimental preparation, *O. tau*, the physical and geometrical parameters in the control condition are approximately m= 1,500 g/cm^4, c~330,000 dyn s/cm^5, k~14,000 dyn/cm^5, and f~1.2 g/cm (Ghanem et al. 1998; Rabbitt et al. 2004).

REFERENCES

ANASTASIO TJ, CORREIA MJ, PERACHIO AA. Spontaneous and driven responses of semicircular canal primary afferents in the unanesthetized pigeon. J. Neurophysiol. 54:335–347, 1985.

ANNIKO M, NORDEMAR H. Formation of the cupula cristae ampullaris: Development in vivo and in vitro. Am. J. Otolaryngol. 3:31–40, 1982.

BAIRD RA, DESMADRYL G, FERNANDEZ C, GOLDBERG JM. The vestibular nerve of the chinchilla. II. Relation between afferent response properties and peripheral innervation patterns in the semicircular canals. J. Neurophysiol. 60:182–203, 1988.

BOYLE R, HIGHSTEIN SM. Resting discharge and response dynamics of horizontal semicircular canal afferents of the toadfish, *Opsanus tau*. J. Neurosci. 10:1557–1569, 1990.

BOYLE R, CAREY JP, HIGHSTEIN SM. Morphological correlates of response dynamics and efferent stimulation in horizontal semicircular canal afferents of the toadfish, *Opsanus tau*. J. Neurophysiol. 66:1504–1521, 1991.

BRICHTA AM, GOLDBERG JM. Afferent and efferent responses from morphological fiber classes in the turtle posterior crista. Ann. N. Y. Acad. Sci. 781:183–195, 1996.

CAMIS M. The Physiology of the Vestibular Apparatus. Oxford, Clarendon, 1930.

CURTHOYS IS. The response of primary horizontal semicircular canal neurons in the rat and guinea pig to angular acceleration. Exp. Brain Res 47(2):286–294, 1982.

DAMIANO ER. A poroelastic continuum model of the cupula partition and the response dynamics of the vestibular semicircular canal. J. Biomech. Eng. 121:449–461, 1999.

DICKMAN JD, CORREIA MJ. Responses of pigeon horizontal semicircular canal afferent fibers. I. Step, trapezoid, and low-frequency sinusoid mechanical and rotational stimulation. J. Neurophysiol. 62:1090–1101, 1989.

DICKMAN JD, REDER PA, CORREIA MJ. A method for controlled mechanical stimulation of single semicircular canals. J. Neurosci. Methods. 25:111–119, 1988.

EZURE K, SCHOR RH, YOSHIDA K. The response of horizontal semicircular canal afferents to sinusoidal rotation in the cat. Exp. Brain Res. 33:27–39, 1978.

FERNÁNDEZ C, GOLDBERG JM. Physiology of peripheral neurons innervating the semicircular canals of the squirrel monkey. II. Response to sinusoidal stimulation and dynamics of peripheral vestibular system. J. Neurophysiol. 34:661–676, 1971.

GHANEM TA, BRENEMAN KD, BROWN HM, RABBITT RD. Ionic composition of inner ear fluids in the oyster toadfish, *Opsanus tau*. Biol. Bull. 214:83–90, 2008.

GHANEM TA, RABBITT RD, TRESCO PA. Three-dimensional reconstruction of the membranous vestibular labyrinth in the toadfish, *Opsanus tau*. Hear Res. 124:27–43, 1998.

GOLDBERG JM, FERNANDEZ C. Physiology of peripheral neurons innervating semicircular canals of the squirrel monkey. I. Resting discharge and response to constant angular accelerations. J. Neurophysiol 34:635–660, 1971.

HIGHSTEIN SM, RABBITT RD, HOLSTEIN GR, BOYLE RD. Determinants of spatial and temporal coding by semicircular canal afferents. J. Neurophysiol. 93:2359–2370, 2005.

HILLMAN DE. Cupular structure and its receptor relationship. Brain Behav. Evol. 10:52–68, 1974.

HILLMAN DE, MCLAREN JW. Displacement configuration of semicircular canal cupulae. Neuroscience. 4:1989–2000, 1979.

HOLSTEIN GR, RABBITT RD, MARTINELLI GP, FRIEDRICH VL, JR., BOYLE RD, HIGHSTEIN SM. Convergence of excitatory and inhibitory hair cell transmitters shapes vestibular afferent responses. Proc. Natl. Acad. Sci. U. S. A. 101:15766–15771, 2004.

HULLAR TE. Semicircular canal geometry, afferent sensitivity, and animal behavior. Anat. Rec. A Discov. Mol. Cell Evol. Biol. 288:466–472, 2006.

LORENTÉ DE NÓ R. Contribucion al estudio matematico del organo del equilibrio. Trabajo publicado en la. 7:202–206, 1927.

LYSAKOWSKI A, GOLDBERG J. Morphophysiology of the vestibular periphery. In: Highstein SM, Popper A, Fay R (eds) The Vestibular System. NY, Springer, 2003.

MARKIN VS, HUDSPETH AJ. Gating-spring models of mechanoelectrical transduction by hair cells of the internal ear. Annu. Rev. Biophys. Biomol. Struct. 24:59–83, 1995.

MCLAREN JW, HILLMAN DE. Displacement of the semicircular canal cupula during sinusoidal rotation. Neuroscience 4:2001–2008, 1979.

O'LEARY DP, HONRUBIA V. Analysis of afferent responses from isolated semicircular canal of the guitarfish using rotational acceleration white-noise inputs. II. Estimation of linear system parameters and gain and phase spectra. J. Neurophysiol. 39:645–659, 1976.

OMAN CM, FRISHKOPF LS, GOLDSTEIN MH. Cupula motion in the semicircular canal of the skate (*Raja erinacea*). Acta Otolaryngol. Stock. 87:528–538, 1979.

OMAN CM, MARCUS EN, CURTHOYS IS. The influence of semicircular canal morphology on endolymph flow dynamics. Acta Otolaryngol. Stock. 103:1–13, 1987.

PAULIN MG, HOFFMAN LF, ASSAD C. Dynamics and the single spike. IEEE Trans. Neural Netw. 15:987–994, 2004.

PETERKA RJ, TOMKO DL. Differences between cats in response properties of horizontal semicircular canal primary afferents. Exp. Brain Res. 56:162–166, 1984.

PETERSON EH, COTTON JR, GRANT JW. Structural variation in ciliary bundles of the posterior semicircular canal. Quantitative anatomy and computational analysis. Ann. N. Y. Acad. Sci. 781:85–102, 1996.

RABBITT RD. Directional coding of three-dimensional movements by the vestibular semicircular canals. Biol. Cybern. 80:417–431, 1999.

RABBITT RD, BOYLE R, HIGHSTEIN SM. Mechanical indentation of the vestibular labyrinth and its relationship to head rotation in the toadfish, Opsanus tau. J. Neurophysiol. 73:2237–2260, 1995.

RABBITT RD, BOYLE R, HIGHSTEIN SM. Influence of surgical plugging on horizontal semicircular canal mechanics and afferent response dynamics. J. Neurophysiol. 82:1033–1053, 1999.

RABBITT RD, BOYLE R, HOLSTEIN GR, HIGHSTEIN SM. Hair-cell versus afferent adaptation in the semicircular canals. J. Neurophysiol. 93:424–436, 2005.

RABBITT RD, DAMIANO ER, GRANT JW. Biomechanics of the semicircular canals and otolith organs. In: Highstein SM, Popper A, Fay R (eds) The Vestibular System. NY, Spirnger, pp. 153–201, 2004.

RAJGURU SM, RABBITT RD. Afferent responses during experimentally induced semicircular canalithiasis. J Neurophysiol. 97:2355–2363, 2007.

RUSCH A, THURM U. Cupula displacement, hair bundle deflection, and physiological responses in the transparent semicircular canal of young eel. Pflugers Arch. 413:533–545, 1989.

SILVER RB, REEVES AP, STEINACKER A, HIGHSTEIN SM. Examination of the cupula and stereocilia of the horizontal semicircular canal in the toadfish *Opsanus tau*. J. Comp. Neurol. 402:48–61, 1998.

STEER RW, LI YT, YOUNG LR, MEIRY JL. Physical properties of the labyrinthine fluids and quantification of the phenomenon of caloric stimulation. Third Symposium on the Role of Vestibular Organs in Space Exploration. Ames: NASA, pp. 409–420, 1967.

STEINHAUSEN W. Über die beobachtungen der cupula in der bognegangsampullen des labyrinthes des libenden hecths. Pfluegers Arch. 232:500–512, 1933.

THÉVENAZ P, UNSER M. A pyramid approach to subpixel registration based on intensity. IEEE Trans. Image Process. 7:27–41, 1998.

VAN BUSKIRK G. Vestibular mechanics. In: Skalak R, Chien S (eds) Handbook of Bioengineering. New York, McGraw Hill, pp. 31.31–31.17, 1987.

WILSON V, JONES G. Mammalian Vestibular Physiology. New York, Plenum, 1979.